NASA TECHNICAL MEMORANDUM

NASA TM X-1001

NASA TM X-1001

ZERO-GRAVITY PERFORMANCE OF [redacted] ULLAGE CONTROL SURFACE WITH LIQUID HYDROGEN WHILE SUBJECTED TO UNSYMMETRICAL RADIANT HEATING

by Kaleel L. Abdalla, Richard A. Flage, and Robert G. Jackson

Lewis Research Center
Cleveland, Ohio

NATIONAL AERONAUTICS AND SPACE ADMINISTRATION • WASHINGTON, D. C. • AUGUST 1964

[redacted]

ZERO-GRAVITY PERFORMANCE OF ULLAGE CONTROL SURFACE WITH LIQUID HYDROGEN WHILE SUBJECTED TO UNSYMMETRICAL RADIANT HEATING

By Kaleel L. Abdalla, Richard A. Flage, and Robert G. Jackson

Lewis Research Center
Cleveland, Ohio

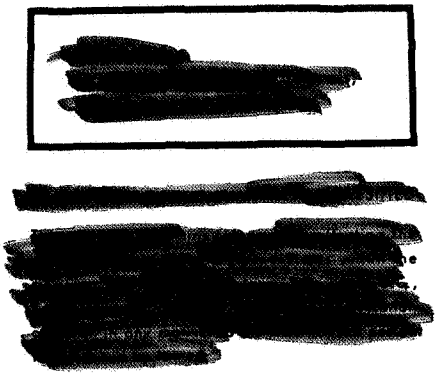

NATIONAL AERONAUTICS AND SPACE ADMINISTRATION

ZERO-GRAVITY PERFORMANCE OF ULLAGE CONTROL SURFACE WITH LIQUID HYDROGEN WHILE SUBJECTED TO UNSYMMETRICAL RADIANT HEATING*

by Kaleel L. Abdalla, Richard A. Flage, and Robert G. Jackson

Lewis Research Center

SUMMARY

The zero-gravity performance of an ullage control surface with liquid hydrogen while subjected to unsymmetrical radiant heating was evaluated by utilizing the Aerobee 150A vehicle during a $4\frac{1}{2}$-minute gravity-free flight.

The results indicate that the standpipe filled successfully and remained full during weightlessness in spite of both adverse heating and small lateral perturbations. Comparison of predicted and measured pressure rise was obtained. Both liquid-hydrogen stratification and Dewar wall drying were observed.

INTRODUCTION

The effects of both zero-gravity environment and solar radiation on high-energy liquid propellants such as liquid hydrogen in a space vehicle orbiting a planet or coasting in outer space pose many problems not readily predictable by computational analyses. The fluid configuration under weightless conditions and the effect of radiation from the celestial body the liquid tank "sees" combine to complicate vehicle requirements, including liquid pumping to restart engines, fluid pressure rise in liquid tanks, location of venting line to relieve excessive pressure buildup, and additional propellant required to account for venting and boiloff.

In an effort to define adequately the fluid configuration and in addition to determine the effects of radiation heat transfer, a program is being conducted by the NASA Lewis Research Center that utilizes zero-gravity time available both from drop towers and from rocket trajectories. Studies of liquid hydrogen in a weightless environment in which the propellant tank was a 9-inch spherical Dewar were made with the Aerobee 150A rocket and are reported in references 1 to 5. The basic zero-gravity configuration of wetting liquids in spherical containers was studied at the Lewis drop tower and is reported in

*Title, Unclassified.

reference 6. Data on positioning the ullage for 3.3-inch-diameter spheres with standpipes were obtained and are reported in references 7 and 8. The investigation reported herein therefore utilized the ullage control principle in an effort to position the liquid at the standpipe with liquid hydrogen in a 9-inch-diameter sphere. The configuration was simultaneously subjected to unsymmetrical radiation heat transfer equivalent to 267 Btu per hour per square foot on one half of the spherical tank and approximately 1 Btu per hour per square foot on the other half. The data were obtained from an instrumented heat-transfer experiment that utilized an Aerobee 150A rocket fired from the NASA Wallops Island Station. The useful zero-gravity time of the flight was $4\frac{1}{2}$ minutes. A film recording the photographic history of the fluid behavior was recovered from the nose-cone camera.

APPARATUS

Experiment and Vehicle Description

A schematic diagram of the liquid-hydrogen experiment and the Aerobee 150A rocket is shown in figure 1. The experiment consisted of a cryogenic Dewar, instrument tower, and recoverable nose cone. Since the Aerobee is a spin-stabilized vehicle, a turntable was provided to nullify the spin rate of the experiment in order to maintain a quiescent fluid environment in the hydrogen Dewar.

After burnout, the vehicle was despun by gas jets to avoid perturbations from inadvertent misalinement of the center of gravity of the nose-cone - payload section and the vehicle.

The camera in the nose cone photographed fluid motion within the hydrogen Dewar for the duration of the flight.

The liquid-hydrogen Dewar (detailed in fig. 2) consisted of a 9-inch-diameter, 0.010-inch-wall, stainless-steel inner sphere within a liquid-nitrogen-cooled 11-inch-diameter vacuum jacket. Details of the design and the construction techniques are the same as those of reference 1. Within the Dewar, as shown in the figure, a 3.25-inch-diameter by 3.8-inch-high cylindrical control surface was mounted to the Dewar wall. Four 1/4-inch cutouts were placed at the base of the standpipe to allow fluid interflow, as shown in figure 2(a).

Within the vacuum space, a 10-inch-diameter spherical copper surface was installed to provide a precalibrated heat input to the hydrogen Dewar. The hemisphere adjacent to the ullage control surface contained electrical heating elements regulated by temperature sensors such that the radiation heat input averaged 267 Btu per hour per square foot. The opposing heater half was a plain copper heat sink with a radiation heat input of 0.6 Btu per hour per square foot.

Instrumentation

In-flight recording of the Dewar and experiment instrumentation was

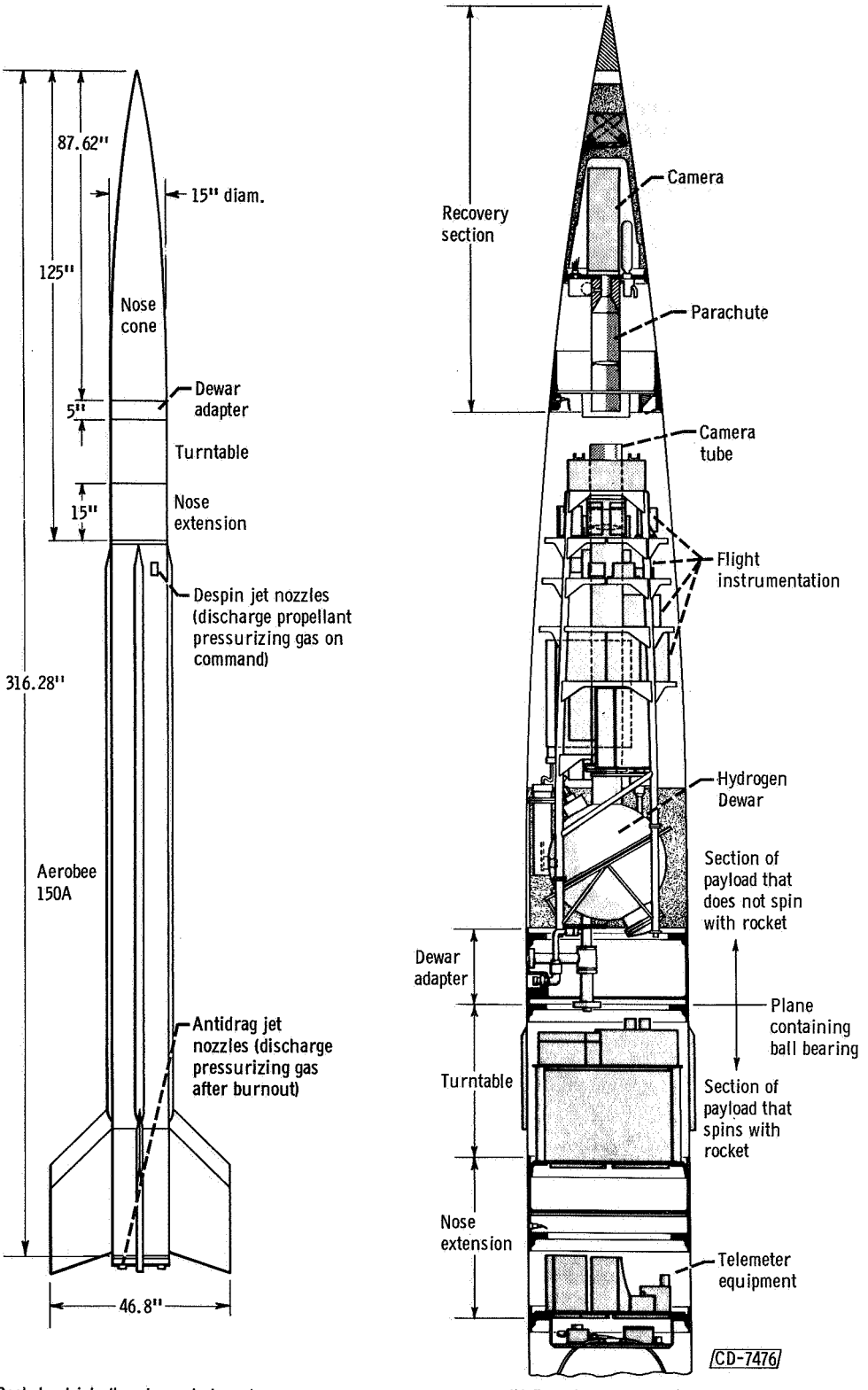

(a) Rocket vehicle (booster not shown).

(b) Experiment and payload.

Figure 1. - Experiment and rocket.

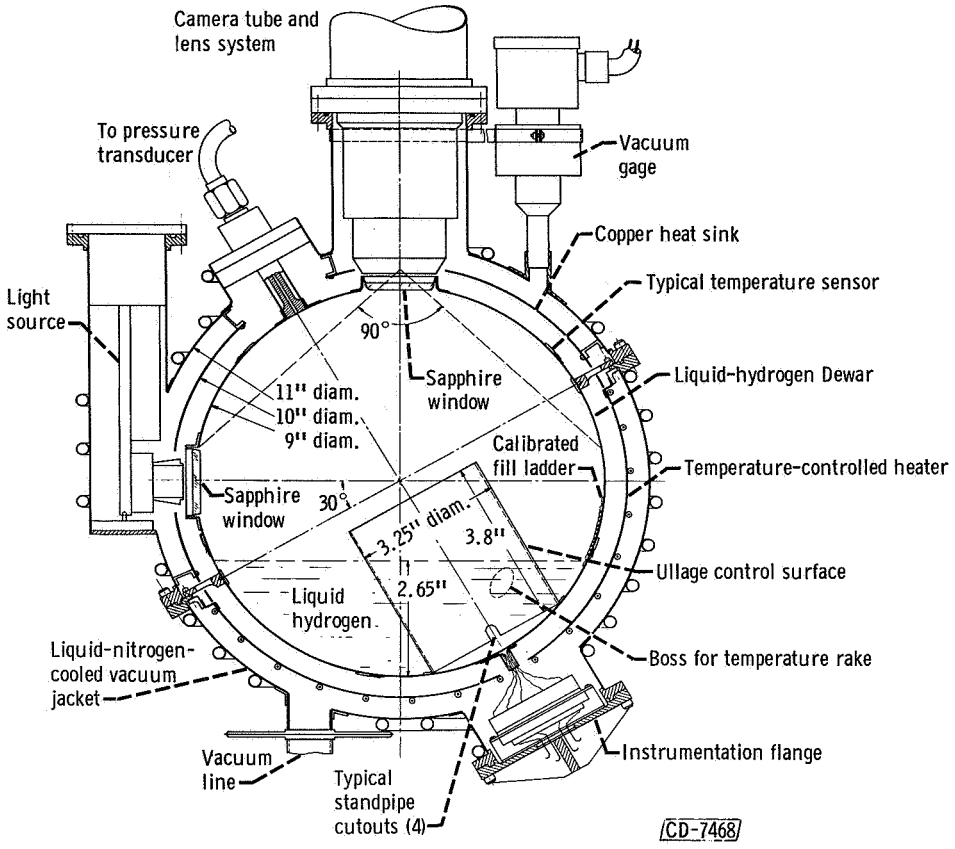

(a) Detailed drawing.

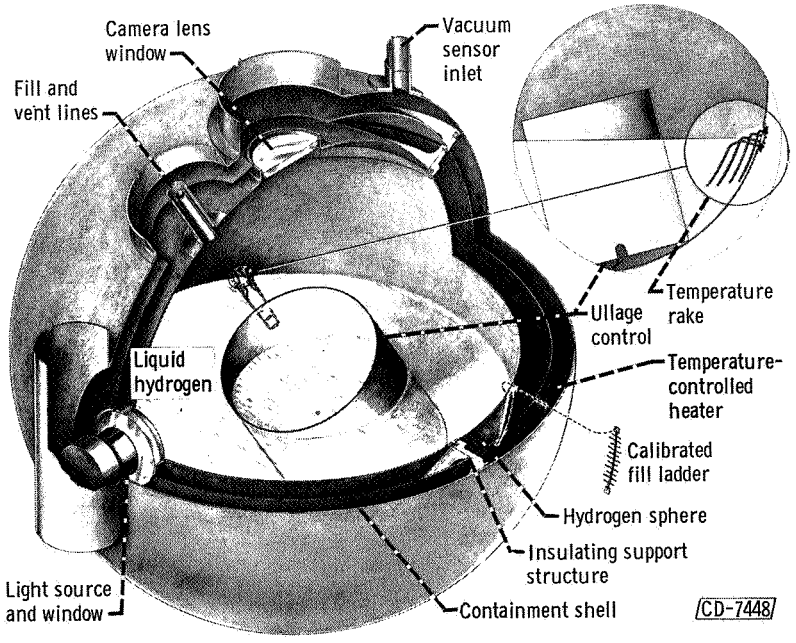

Rake element	Distance from wall, in.
A	0.088
B	.262
C	.465
D	.672

(b) Cutaway drawing, including rake details.

Figure 2. - Liquid-hydrogen Dewar.

accomplished by the electronic measuring systems located in the flight instrumentation section shown in figure 1. Commutated and continuous channels of information were transmitted by the telemeter equipment (see fig. 1) to ground receiving stations.

The Dewar wall temperatures were measured by means of 10 platinum-resistance temperature transducers, located as shown in figure 3. Characteristics of these sensors are described in reference 1. A composition resistor rake was used to measure the temperature profile from the wall to the bulk of the hydrogen. This rake, shown in figure 2(b), consisted of four 1/10-watt miniature composition resistors spaced from the Dewar wall as listed in the table on that figure. Temperatures of both the electrically controlled heater and the heat sink were obtained from two platinum-resistance sensors located on each hemisphere.

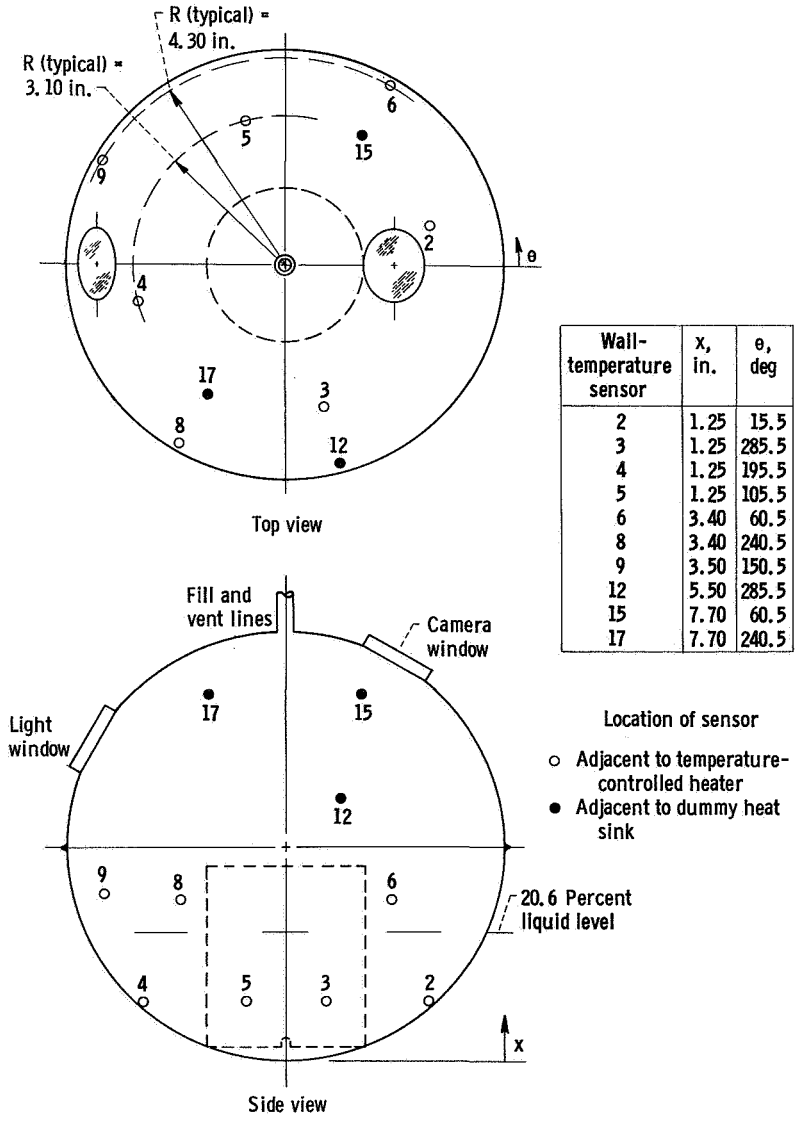

Wall-temperature sensor	x, in.	θ, deg
2	1.25	15.5
3	1.25	285.5
4	1.25	195.5
5	1.25	105.5
6	3.40	60.5
8	3.40	240.5
9	3.50	150.5
12	5.50	285.5
15	7.70	60.5
17	7.70	240.5

Figure 3. - Location of hydrogen sphere temperature sensors.

Hydrogen Dewar pressure was monitored by means of a pressure transducer with its voltage output precalibrated to a known pressure history.

The gravity level of the experiment was monitored by accelerometers located at each of the vehicle's axes. In addition, a 2-inch-diameter glass sphere partly filled with mercury was used as a gravity indicator, the image of which was superimposed on the motion-picture film.

The vehicle trajectory was obtained from ground radar tracking.

Data Reduction

All telemetered data tapes were digitized and programed into the Lewis Research Center automatic data processing system according to predetermined voltage-output calibrations. The method of

calculating the heat-transfer results is presented herein.

PROCEDURE

Several hours prior to scheduled launch, the experiment precountdown was begun. Subject to specified vacuum conditions, the hydrogen Dewar was cryogenically cooled by flowing liquid nitrogen through the vacuum-jacket coolant lines. Shortly thereafter, the experiment container was filled with liquid hydrogen above the 80-percent level, which augmented the Dewar cool down and established the hydrogen boiloff rate. During this time, the experiment instrumentation was continuously monitored.

At 150 minutes prior to scheduled launch, the countdown was initiated. Final calibrations of sensors and transducers were recorded, and the liquid level of the experiment was set so that the estimated level at lift-off would be 30 percent by volume. Then the experiment was integrated with the vehicle and the nose cone. For this flight, as a result of minor holds at launch time, the experiment was flown with a liquid level of 20.6 percent.

FLIGHT CHARACTERISTICS

The primary vehicle functions and experiment programed commands are shown in figure 4, which describes the vehicle trajectory, obtained from radar tracking. Fifteen seconds after lift-off, the experiment camera was started. Also at this time, power to the electrically controlled radiation heater was initiated. After sustainer burnout at 52 seconds after lift-off, the vehicle coasted in a reduced gravity environment until the start of despin at 76 seconds after lift-off. During this interval between 52 and 76 seconds, atmospheric drag on the vehicle was counteracted by thrust augmentation obtained by flowing residual oxidizer tank pressurization gas out of the engine nozzle. The antidrag thrust decay closely approximated the drag decay. At 76 seconds after lift-off, then, the oxidizer tank shutoff valve was closed and thus further thrusting was stopped. At the same time the vehicle casing was despun by flowing residual helium gas from the fuel tank out of the despin jet nozzles (see fig. 1(a), p. 3). The vehicle

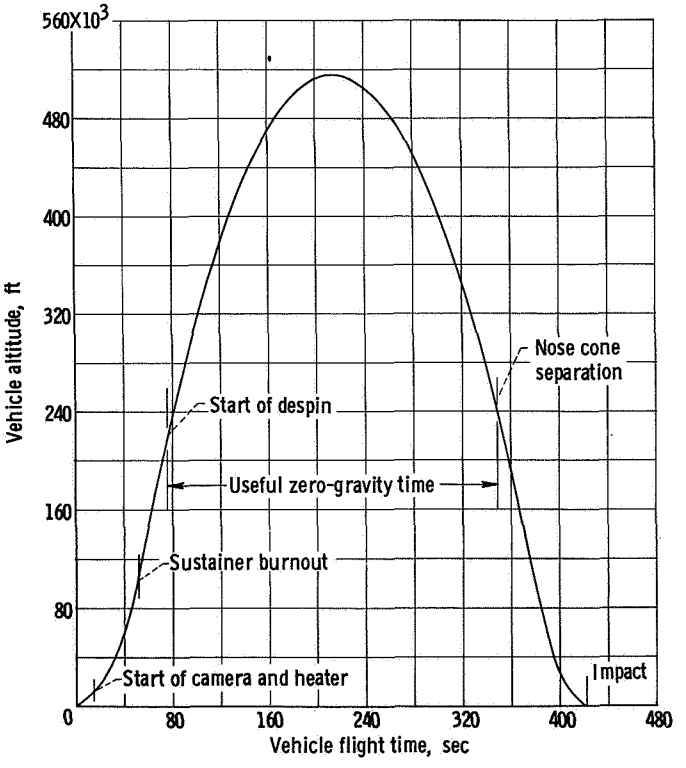

Figure 4. - Vehicle flight trajectory, including programed functions.

continued to coast until 350 seconds after lift-off, at which time the recoverable nose cone was separated from the vehicle. At 422 seconds the nose cone impacted into the Atlantic Ocean. Within minutes the nearby helicopter recovery team located the floating nose cone.

The resulting useful zero-gravity time, as shown in figure 5(a), was that flight time during which the acceleration rate in the thrust axis was no greater than 0.001 g. This period, from 76 to 349 seconds after lift-off, is also indicated in figure 4.

Lateral Acceleration Perturbation

Because the Aerobee 150A rocket is spin stabilized at a nominal rate of 2.5 rps, a despin mechanism was employed for the entire payload to counteract

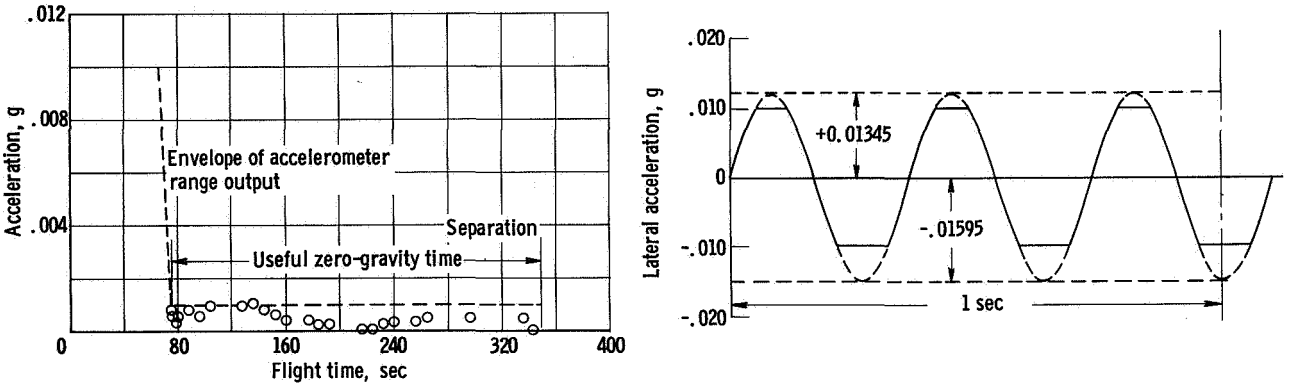

(a) Thrust axis, 0.010-g accelerometer.

(b) Lateral acceleration perturbation; ±0.010-g accelerometer; frequency, 2.73 cps; average amplitude, ~0.0147 g.

Figure 5. - Experiment acceleration field.

the rotational acceleration of the vehicle. With correct operation the fluid within the Dewar would have experienced no rotational or lateral excitations. A malfunction in the vehicle despin system occurred during flight, however, such that a lateral acceleration perturbation was imparted to the Dewar throughout the weightless time. Average equivalent perturbation acceleration was ±0.015 g at a frequency of 2.73 cps. A graphic representation of the data obtained in the axis of rotation is shown in figure 5(b). Because the accelerometer used was overranged, the amplitude was extrapolated from the telemetered traces.

DISCUSSION OF RESULTS

Ullage Control Effectiveness

Based on drop-tower studies (ref. 7), the fluid configuration during weightlessness for the spherical Dewar and the standpipe utilized in the experiment should be that of a fluid-filled standpipe with the bulk of the remaining liquid located near the base of the control surface. The effect of a high-radiation heat input adjacent to the ullage surface, however, is to drive

the fluid away from the source of heat, that is, away from the control surface. Furthermore, because of the despin malfunction described earlier, the fluid was subjected to a lateral acceleration, which tended to concentrate the liquid into a plane approximately 60° to the axis of the standpipe. The amplitude of the perturbation was on the average ±0.015 g at a frequency of 2.73 cps.

The standpipe did fill as shown by the photographic sequences of figure 6 in spite of both adverse heating and acceleration perturbations. The time required under these conditions was of the order of 1 minute. This time to fill was long compared with that of the drop-tower studies (ref. 7) because of the relatively small holes at the bottom of the standpipe. As the photographs indicate, the control was liquid filled for the remainder of the zero-gravity

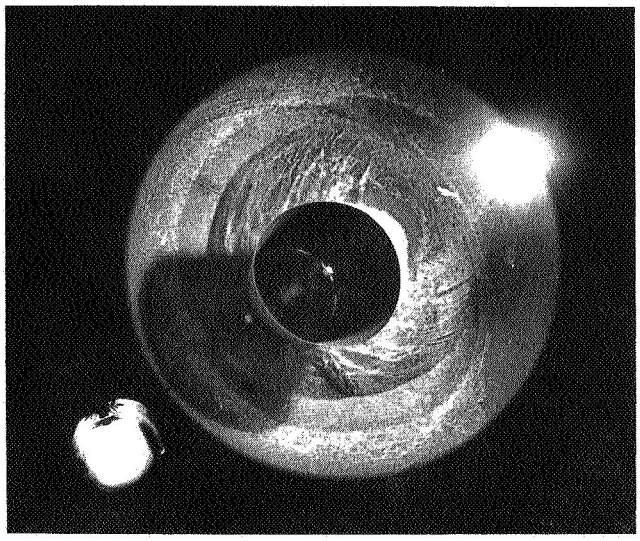

(a) Flight time, 13 seconds.

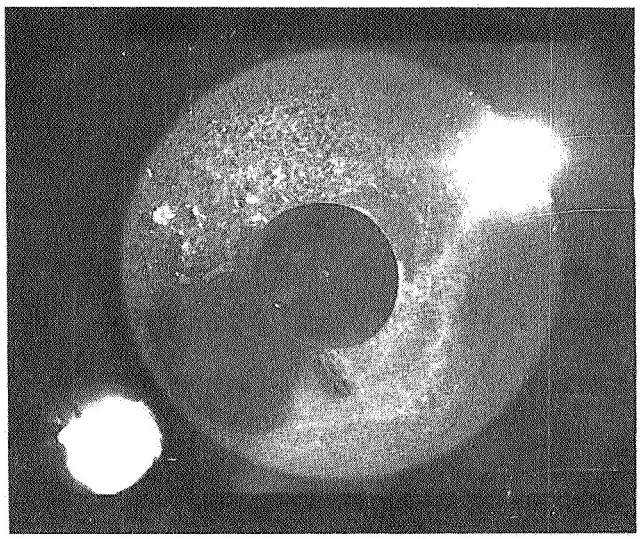

(b) Flight time, 79 seconds. (Start of zero-gravity time, 76 sec.)

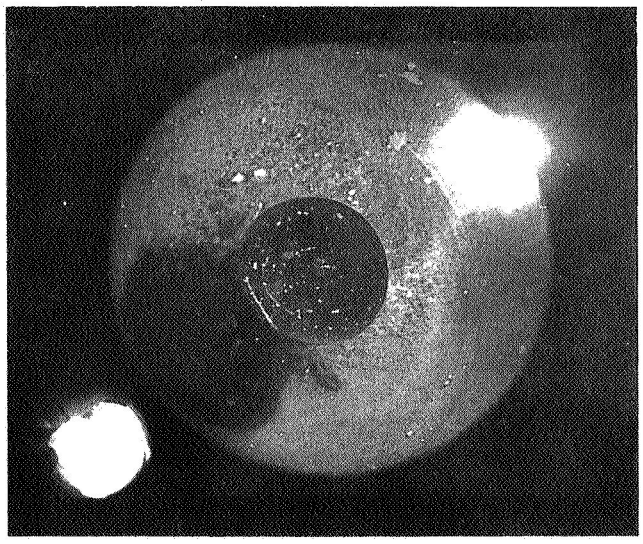

(e) Flight time, 159 seconds.

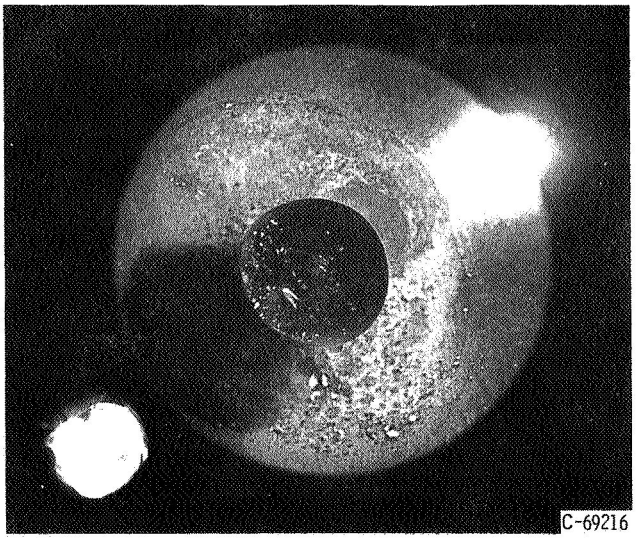

(f) Flight time, 221 seconds.

Figure 6. - Photographic sequence showing ullage

time, while most of the excess was contained in the annulus at the base of the standpipe.

The complete motion-picture sequence showing this process in flight is in the film supplement of reference 5.

Heat-Transfer Characteristics

The total amount of heat absorbed by the liquid hydrogen is equivalent to the heat transferred to the hydrogen by radiation plus the heat leaks minus the heat stored in the Dewar wall, that is,

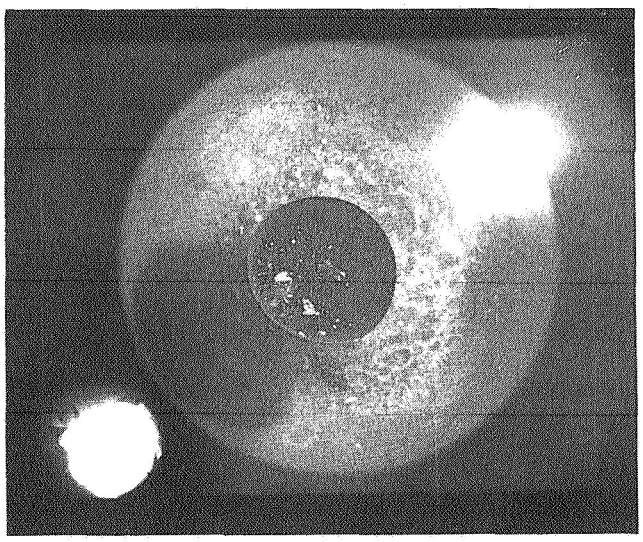

(c) Flight time, 135 seconds.

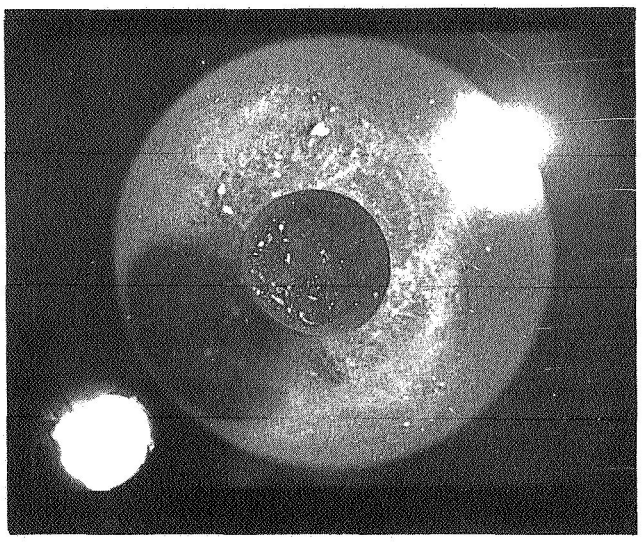

(d) Flight time, 144 seconds.

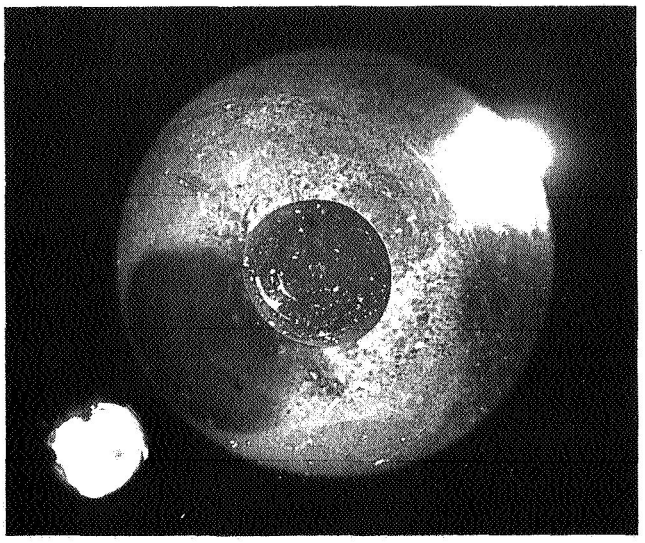

(g) Flight time, 240 seconds.

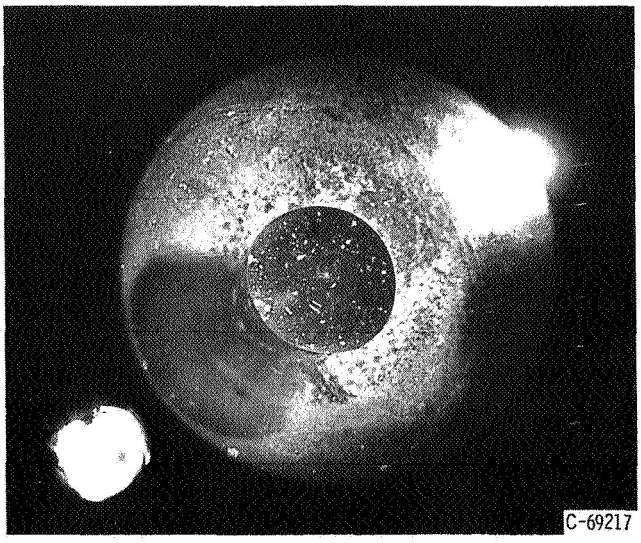

(h) Flight time, 260 seconds.

control filling process in zero-gravity environment.

$$\Delta Q_{abs} = q_r \Delta t + q_{hl} \Delta t - \Delta Q_s$$

where

Q_{abs} total amount of heat absorbed by liquid hydrogen, Btu

q_r net rate of radiant energy, Btu/hr

t time, hr

q_{hl} heat leak energy rate, Btu/hr

Q_s heat stored in Dewar wall, Btu

The heat transferred by radiation was computed from the following equation, which was obtained from reference 9, section 5-5:

$$q_{r_j} = \sum_{i=1}^{n} B_{ij} W_i A_i - W_j A_j$$

where

q_{r_j} net rate of radiant energy gained by surface j

B_{ij} absorption factor between surfaces i and j

W total hemispherical emissive power per unit area

A surface area

The development of the respective parameters for this equation are detailed in the reference. The application to this particular experiment, however, is not presented herein. The heat leaks and the heat stored in the Dewar wall were computed with techniques similar to those presented in reference 1.

The radiation-heater-temperature history measured during flight is presented in figure 7. From this profile for the time period and from emissivities obtained for a similar heat-transfer model of reference 1, the radiated heat rate was obtained by accumulating the integrated heat rates over the weightless period of flight. In order to eliminate flight time as a parameter, the hydrogen sphere pressure, the time history of which is given in figure 8, is presented as a function of heat added in figure 9. Included for comparison are lines depicting the pressure rise as a function of heat input that may be calculated based on certain assumptions about the heat distribution in the Dewar. The homogeneous-mixing line is calculated by using the tables of reference 10, with the heat assumed to be distributed uniformly on a mass basis between the liquid and the gas. The surface-evaporation line is calculated by using reference 10, with the assumption that all the incoming heat evaporates liquid.

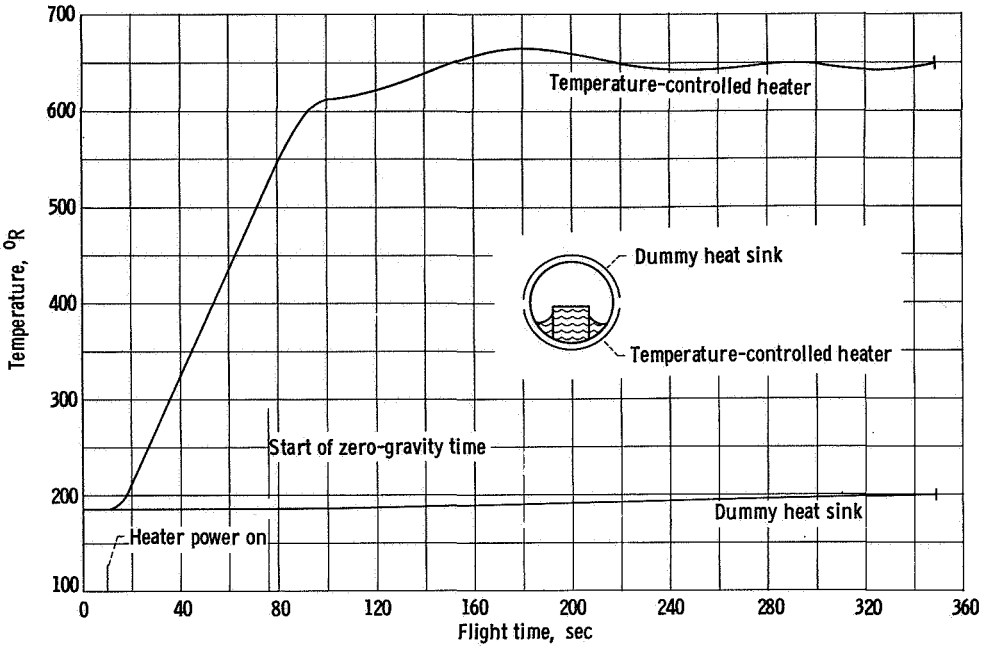

Figure 7. - Temperature rise of radiation heaters.

As shown in figure 9(a), the actual pressure rise was somewhat higher than that predicted by assuming homogeneous mixing during the early portion of weightlessness and continued to deviate at an increasing rate for the remainder of the flight. The deviation from the calculations based on homogeneous mixing and surface evaporation is graphically represented in figure 9(b), shown as a percentage between the surface-evaporation line and the curve for homogeneous mixing. As the figure shows, little change was observed during the first portion of the flight, with values ranging from $22\frac{1}{2}$ to approximately 24 percent pressure deviation. During the latter portion, however, the actual pressure deviated at an increasing rate and reached a deviation of 66 percent at the end of the flight.

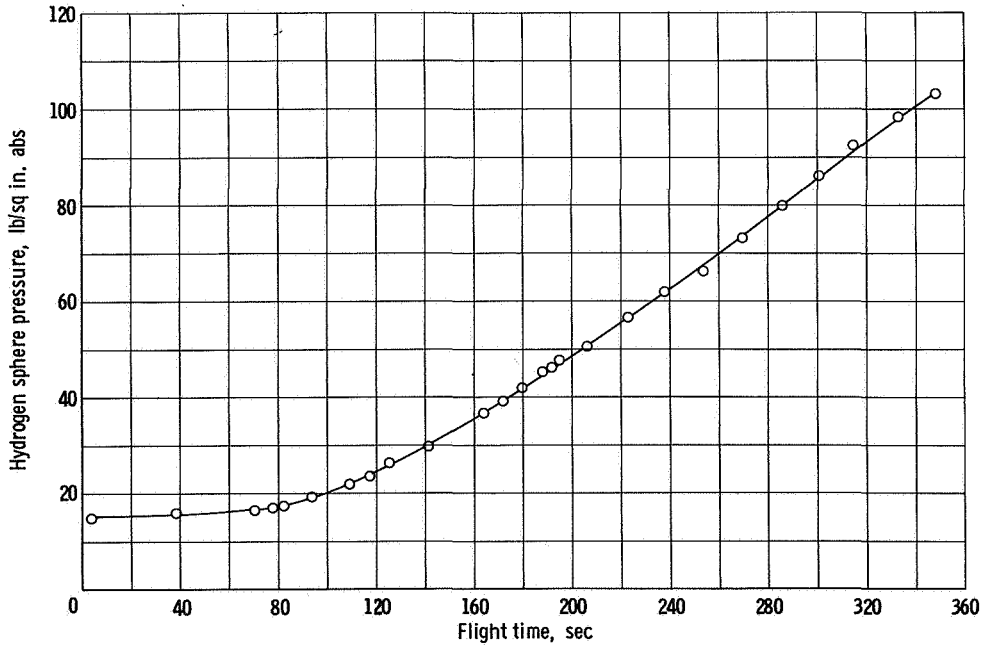

Figure 8. - Pressure rise in hydrogen sphere during flight.

The following postulation is presented as an explanation of the phenomena occurring during this experiment. Prior to initiation of weightlessness, the liquid configuration was similar to that in a gravitational field; that is, the liquid was

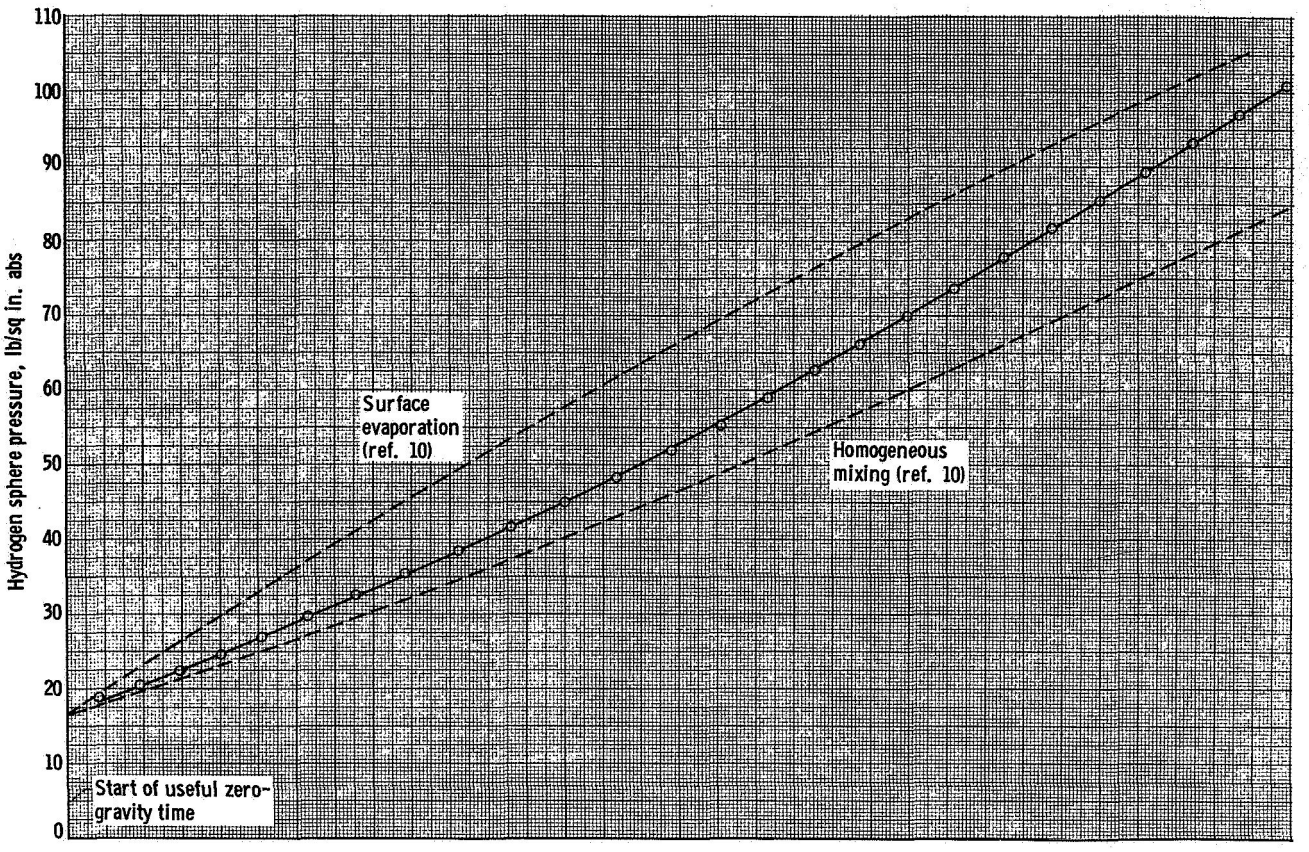

(a) Comparison of actual pressure rise to calculated values for surface evaporation and for homogeneous mixing.

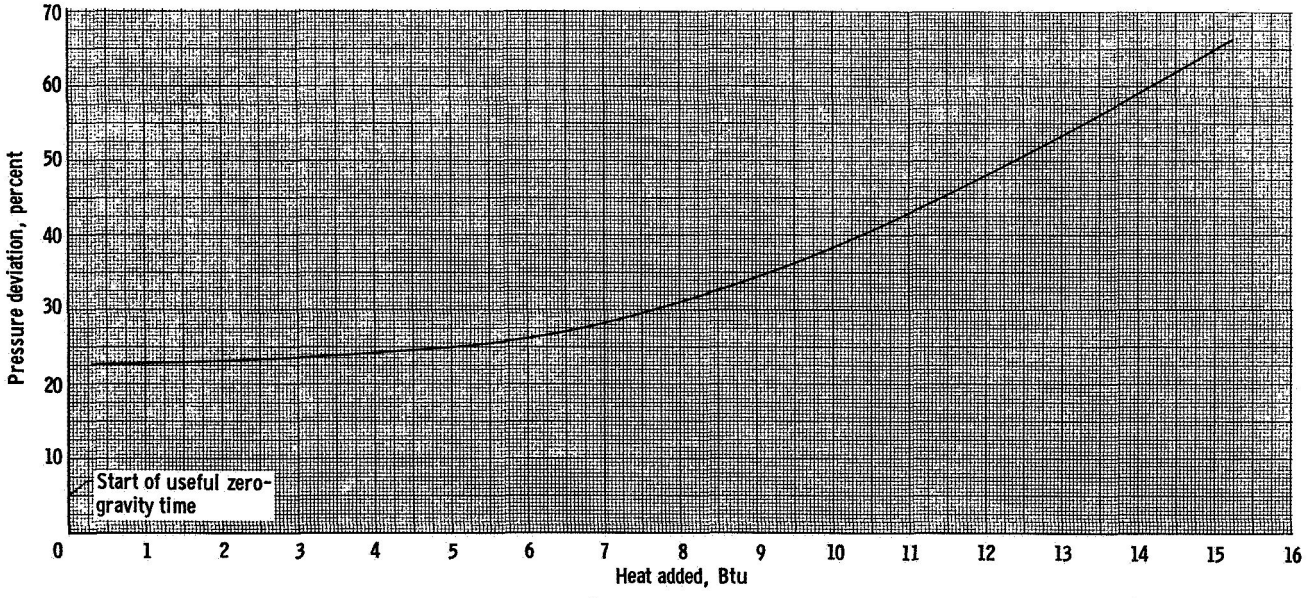

(b) Percentage deviation of actual pressures from surface evaporation and homogeneous values. Pressure deviation: (actual pressure - homogeneous pressure)/(surface evaporation pressure - homogeneous pressure) x 100; values taken from figure 9(a).

Figure 9. - Pressure-rise characteristics with heat addition during weightlessness.

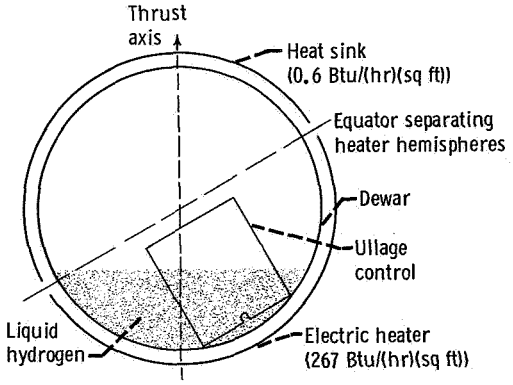

(a) Normal gravity environment.

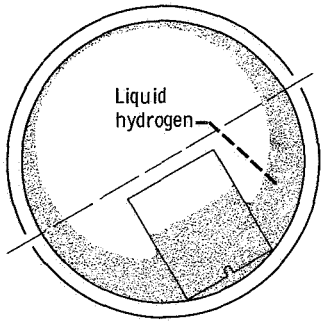

(b) Partly full standpipe.

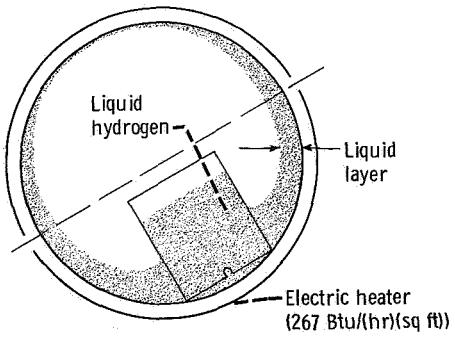

(c) Nearly full standpipe.

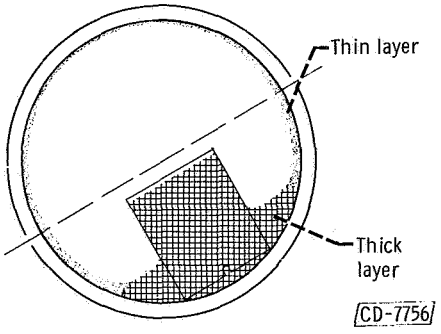

(d) Full standpipe.

Figure 10. - Liquid configuration.

contained in a pool as shown in figure 10(a). As the gravitational environment quickly reduced to near weightlessness, the fluid position was dictated by surface tension forces such that the liquid began wetting the Dewar wall and at the same time began filling the ullage control by capillary action. The configuration at this time was similar to that of figure 10(b). During the first minute of weightlessness (the time required to fill the standpipe), a considerable liquid layer was present along the Dewar wall for the hemisphere containing the ullage control (see fig. 10(c)). This hemisphere was exposed to the high radiation temperature environment of 267 Btu per hour per square foot. The bubbles created by nucleate boiling were, for the most part, condensed by the relatively thick layer of hydrogen. By the end of the first minute of weightlessness, however, the liquid completely filled the standpipe, as described earlier. At that time the configuration consisted of a deep layer in the standpipe, a relatively thick layer near the base of the standpipe, and a thin layer near the Dewar equator (see fig. 10(d)). For this configuration, then, it is expected that the liquid in the standpipe and near its base (crosshatched area in fig. 10(d)) was of sufficient depth to continue the condensing process. Since this configuration remained throughout the weightless period, the condensing process should have remained unchanged. Furthermore, condensation of the bubbles suggests subcooling of the liquid. Subcooling of the liquid was, in fact, measured by the temperature profile rake. The data presented in figure 11 indicate that about 1° R of subcooling was established within 1 minute after the beginning of weightlessness and remained for the duration of flight.

For the thin liquid layer (dotted area of fig. 10(d)) adjacent to the high-temperature heater, the bubbles did not condense but delivered their heat to the gas ullage. This process raises the pressure at a rate near that for surface evaporation. A subcooled liquid, on the other hand, predicts pressures lower than those for homogeneous mixing. The net effect, then, during this 1-minute period in which the actual pressure rose from 16.5 to 30 pounds per square inch absolute was a pressure above that for homogeneous mixing that ranged from 22.5 to 24 percent of that obtained by total surface evaporation.

During the next 2 minutes of weightless time, additional heat was carried to the gas ullage where the hydrogen layer was thin (dotted area of fig. 10(d)), while the subcooled liquid remained unchanged (fig. 11). The pressure deviation curve indicated this effect, as the pressure continually deviated at an increasing rate and reached 45 percent (fig. 9(b)) during this time.

For the remainder of the flight this thin film of hydrogen began drying as observed in the motion pictures (film supplement, ref. 5) and by the response of the respective surface temperature sensors. During this time, heat was added directly to the gas ullage, and the pressure began to approach that predicted by surface evaporation (fig. 9(a)). This effect is more graphically illustrated in figure 9(b), where the deviation has increased to 66 percent by the end of the weightless period.

Wall-Drying Phenomenon

The drying process observed in the motion-picture film is shown in fig-

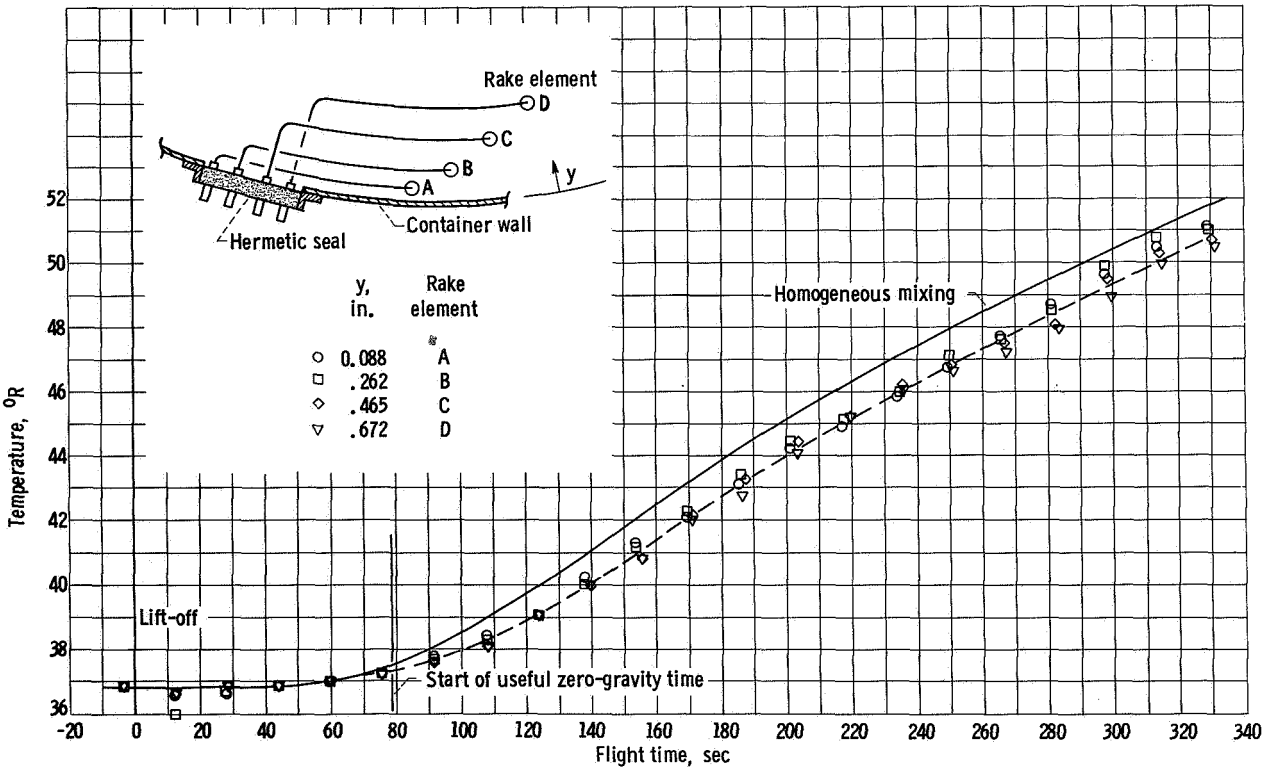

Figure 11. - Liquid-hydrogen temperature profile near wall adjacent to temperature-controlled heater.

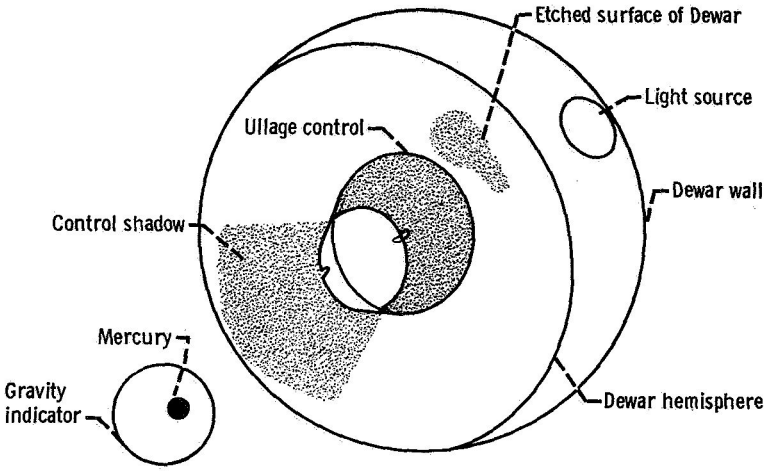

Orientation sketch

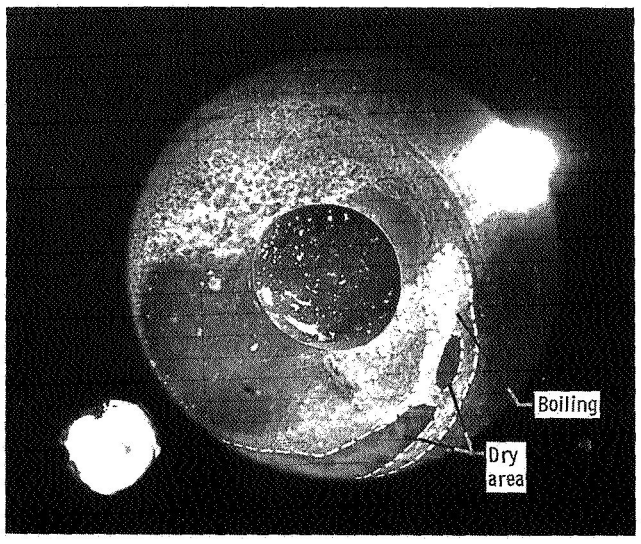

(c) Flight time, 301 seconds.

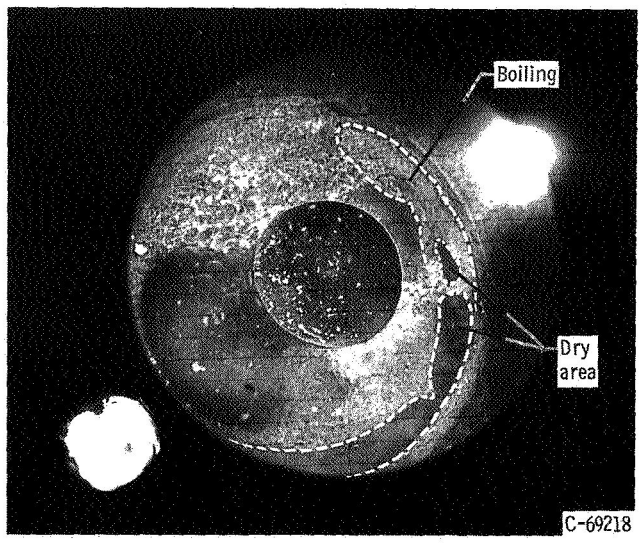

(d) Flight time, 314 seconds.

Figure 12. - Photographic sequence showing wall drying adjacent